molecules

MDPI

Article

Structural Evolution of Small-Sized Phosphorus-Doped Boron Clusters: A Half-Sandwich-Structured PB_{15} Cluster

Danyu Wang, Yueju Yang, Shixiong Li * and Deliang Chen

School of Physics and Electronic Science, Guizhou Education University, Guiyang 550018, China; 18508507005@163.com (D.W.); yangyueju1003@163.com (Y.Y.); chendeliang@gznc.edu.cn (D.C.)
* Correspondence: lishixiong@gznc.edu.cn

Abstract: The present study is a theoretical investigation into the structural evolution, electronic properties, and photoelectron spectra of phosphorus-doped boron clusters $PB_n^{0/-}$ (n = 3–17). The results of this study revealed that the lowest energy structures of PB_n^- (n = 3–17) clusters, except for PB_{17}^-, exhibit planar or quasi-planar structures. The lowest energy structures of PB_n (n = 3–17), with the exceptions of PB_7, PB_9, and PB_{15}, are planar or quasi-planar. The ground state of PB_7 has an umbrella-shaped structure, with C_{6V} symmetry. Interestingly, the neutral cluster PB_{15} has a half-sandwich-like structure, in which the P atom is attached to three B atoms at one end of the sandwich, exhibiting excellent relative and chemical stability due to its higher second-order energy difference and larger HOMO–LUMO energy gap of 4.31 eV. Subsequently, adaptive natural density partitioning (AdNDP) and electron localization function (ELF) analyses demonstrate the bonding characteristics of PB_7 and PB_{15}, providing support for the validity of their stability. The calculated photoelectron spectra show distinct characteristic peaks of PB_n^- (n = 3–17) clusters, thus providing theoretical evidence for the future identification of doped boron clusters. In summary, our work has significant implications for understanding the structural evolution of doped boron clusters $PB_n^{0/-}$ (n = 3–17), motivating further experiments regarding doped boron clusters.

Keywords: boron clusters; phosphorus-doped; geometrical structures; spectra

Citation: Wang, D.; Yang, Y.; Li, S.; Chen, D. Structural Evolution of Small-Sized Phosphorus-Doped Boron Clusters: A Half-Sandwich-Structured PB_{15} Cluster. *Molecules* **2024**, *29*, 3384. https://doi.org/10.3390/molecules29143384

Academic Editor: Zbigniew Jan Leśnikowski

Received: 30 May 2024
Revised: 12 July 2024
Accepted: 16 July 2024
Published: 18 July 2024

1. Introduction

It is well known that boron is a naturally abundant element, and scientists have been exploring the properties and applications of boron, boron compounds, and their derivatives [1–5]. With the successive discoveries of fullerene C_{60}, carbon nanotubes, and graphene [6–8], carbon nanomaterials have attracted considerable attention and become a dynamic field of research; similarly, as a neighbor of carbon, boron has also received significant attention from researchers. Boron compounds exhibit intrinsic electronic defects, as well as the ability to form an outstanding number of multicenter bonds, which endow them with rich structural features and chemical properties [9–14]. The groundbreaking discovery of borospherene [15] in 2014 sparked extensive research on boron clusters [16–22]. Over the past two decades, a great deal of theoretical and experimental research has focused on the geometric structure and electronic characteristics of bare boron clusters [23]. It is generally believed that bare boron clusters exhibit planar or quasi-planar geometric shapes over a large range of sizes. One of the most important discoveries is the planar B_{36}^- cluster [24], a highly stable cluster with central hexagonal vacancies that can be synthesized on a metal substrate to form "borophene". The experimental discoveries of borospherene and borophene provide new insights into novel boron nanomaterials and nanodevices.

Over the past decade, scientists have investigated richly doped boron clusters, with a primary focus on doping single metal atoms into boron clusters of various sizes. Metal doping is an effective method for adjusting the chemical bonds and occupied energy levels of boron clusters through the addition of metal elements, thereby changing their

physicochemical properties. Doping metal atoms into boron clusters can lead to the formation of new geometric configurations and chemical properties, such as ring-like, sandwich-like, tube-like, and cage-like structures [17,19,20,25–34]. Following the doping of single alkali metal atoms into the quasi-planar structures of B_{20}^- and B_{22}^- [35], species including LiB_{20}^-, NaB_{22}^-, and KB_{22}^- exhibit bi-ring structures [33,36]. Quasi-planar B_{12}^- clusters, upon doping with single transition metal atoms of Co, Rh, or Ta, exhibit half-sandwich structures [10,37,38]. Doping with single transition metal atoms can modify the bi-ring tubular B_{24} into cage-like boron clusters (TiB_{24}, VB_{24}, and MnB_{24}) and tri-ring tubular doped boron clusters (ScB_{24}) [39–41], or convert quasi-planar B_{24}^- into cage-like boron clusters (TiB_{24}^-, CrB_{24}^-, and VB_{24}^-) [35,42].

Compared with metal-doped boron clusters, there is relatively little research on the doping of boron clusters with non-metal atoms [43–47]. In particular, there have been few studies on the structural evolution of boron clusters with the addition of phosphorus atoms. The recently reported P-doped boron cluster $P_2B_{12}^{+/0/-}$ has the same cage structure, with D_{3h} symmetry [46]. The theoretical study of phosphorus-doped small boron clusters is of great significance for the discovery of new structures and properties of boron clusters. In this study, the effect of P-atom doping on the structure and electronic properties of boron clusters $B_n^{0/-}$ (n = 3–17) was investigated through employment of the particle swarm optimization (CALYPSO) method [48] and the density-functional theory method PBE0 [49].

2. Results and Discussion

2.1. Geometric Configurations

Early theoretical and experimental studies found that anionic boron clusters with an atomic numbers less than 37 always maintain quasi-planar or planar structures; however, while some neutral boron clusters do have quasi-planar or planar structures, others have tube or cage-like structures. The structures of boron clusters change after atom doping. In order to facilitate understanding via visualization, the low-lying isomers of $PB_n^{0/-}$ (n = 3–17), along with their corresponding relative energy values, are displayed in Figures S1–S30, and the lowest energy structures of $PB_n^{0/-}$ (n = 3–17) are depicted in Figures 1 and 2. Clear structural diagrams show that the lowest-lying energy structures of PB_n^- (n = 3–17) clusters have planar or quasi-planar structures, except for PB_{17}^-. The lowest energy structures of PB_n (n = 3–17) are planar or quasi-planar, with the exceptions of PB_7, PB_9, and PB_{15}. As can be observed in Figures 1 and 2, after the addition of the P atom, most boron clusters remain virtually unchanged from their corresponding bare boron cluster forms, such as PB_n (n = 3–6, 8, 10, 12) and PB_n^- (n = 3, 5–8, 10–16) [23,50,51]. In order to further discuss the structural changes of boron clusters, we also compared their structures after replacing a boron atom with a phosphorus atom, and without replacing the boron atom. Compared with the bare boron clusters $B_n^{0/-}$ (n = 4–18), the structures of most $PB_{n-1}^{0/-}$ (n = 4–18) clusters changed, except for those of PB_3^-, PB_3, PB_4, and PB_5 (which remained almost similar to those of B_4^-, B_4, B_5, and B_6, respectively); that is, the structures of the bare boron clusters changed due to the replacement of one atom with a P atom. The lowest energy configurations of $PB_n^{0/-}$ (n = 3, 5, 6, 8) are planar structures, with the P atom attached to the boron atoms of the bare boron clusters $B_n^{0/-}$ (n = 3, 5, 6, 8) [50]. The lowest-lying energy structures of $PB_n^{0/-}$ (n =10, 12) are quasi-planar, similar to the ground-state structures of their corresponding bare boron clusters, $B_{10}^{0/-}$ and $B_{12}^{0/-}$, with the addition of a phosphorus atom bonded to the boron atoms. PB_{10}^- has a chiral symmetrical structure. Likewise, the planar clusters PB_4, PB_7^-, PB_{11}^-, PB_{13}^-, and PB_{14}^-, as well as the quasi-planar cluster PB_{16}^-, have similar structures to those of their corresponding bare boron clusters [23,50]. However, the ground-state structures of the planar PB_4^- and quasi-planar PB_{11}, PB_{13}, and PB_{16} clusters are different from their corresponding bare boron clusters due to the action of the P atom.

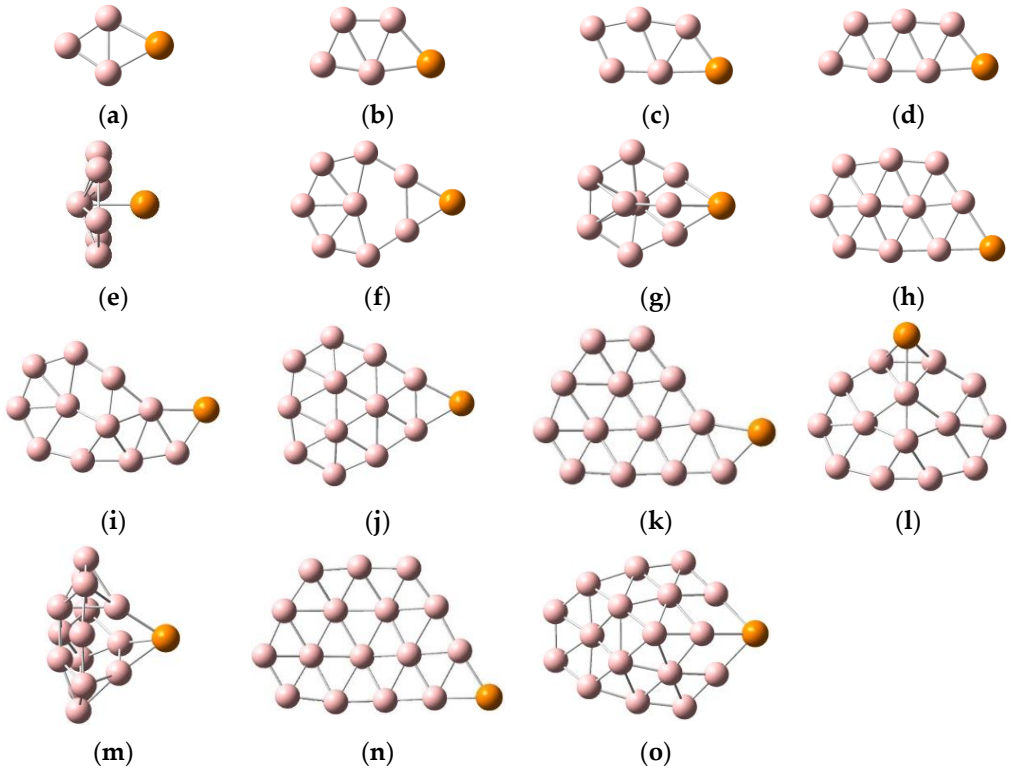

Figure 1. Structures of PB_n, where pink balls represent boron atoms and orange ball represents phosphorus atom. (**a**) PB_3 C_{2V}; (**b**) PB_4 C_S; (**c**) PB_5 C_S; (**d**) PB_6 C_S; (**e**) PB_7 C_{6V}; (**f**) PB_8 C_{2V}; (**g**) PB_9 C_S; (**h**) PB_{10} C_1; (**i**) PB_{11} C_1; (**j**) PB_{12} C_S; (**k**) PB_{13} C_1; (**l**) PB_{14} C_S; (**m**) PB_{15} C_S; (**n**) PB_{16} C_1; (**o**) PB_{17} C_S.

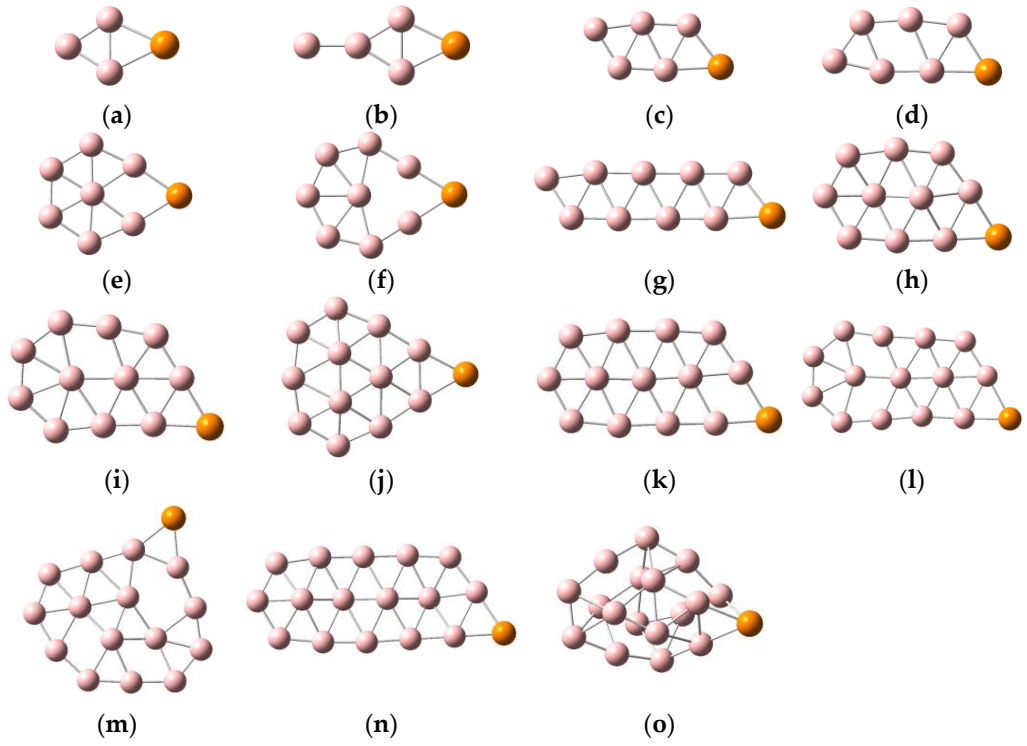

Figure 2. Structures of PB_n^-, where pink balls represent boron atoms and orange ball represents phosphorus atom. (**a**) PB_3^- C_{2V}; (**b**) PB_4^- C_{2V}; (**c**) PB_5^- C_S; (**d**) PB_6^- C_S; (**e**) PB_7^- C_{2V}; (**f**) PB_8^- C_{2V}; (**g**) PB_9^- C_S; (**h**) PB_{10}^- C_1; (**i**) PB_{11}^- C_S; (**j**) PB_{12}^- C_S; (**k**) PB_{13}^- C_1; (**l**) PB_{14}^- C_S; (**m**) PB_{15}^- C_1; (**n**) PB_{16}^- C_1; (**o**) PB_{17}^- C_1.

The planar wheel-shaped structure of B_9 becomes the three-dimensional structure of PB_9 with the doping of a P atom; the anion cluster B_9^-, with a similar structure, changes from the planar wheel to the double-chain planar structure of PB_9^-. The lowest energy configurations of PB_{14} and PB_{17} have quasi-two-dimensional structures, and PB_{17}^- has a three-dimensional cage-shaped structure. It is important to note the specific behaviors of PB_7, PB_9^-, and PB_{13}. For the PB_9^- cluster, at the PBE0/6-311+G(d) level, the double-chain planar structure (Figure S14a) is more stable than the planar structure (Figure S14b), with an energy gap of 0.17 eV. At the higher level, CCSD(T)/6-311+G(d)//PBE0/6-311+G(d)+ZPE (zero-point energy corrections), both structures are almost degenerate in regards to energy, each with a tiny energy gap (that is, the planar structure (Figure S14b) is more stable than the double-chain planar structure (Figure S14a), with an energy gap of 0.01 eV). We consider the double-chain structure as the lowest energy structure of PB_9^-; the same is true for the PB_7 and PB_{13} clusters. It is worth mentioning that the umbrella-like structure found in PB_7 is also the lowest energy structure in many metal-doped boron clusters, such as LiB_7, $BeB_7^{0/-}$, $BeB_8^{0/-}$, and MgB_8 [52–54]. Research shows that the low-valent actinide(III) boron clusters AnB_7 (An = Pa, U, Np, and Pu), with umbrella-shaped structures, exhibit high electronic stability and can be obtained in the gas phase at room temperature [55]. Similarly, the neutral cluster PB_7 also has an umbrella-shaped structure, with C_{6v} symmetry. Therefore, in this study, we will highlight the umbrella-like structure of PB_7, which can provide a theoretical basis for the design of highly stable boron-based nanomaterials. In addition, the quasi-planar structure of B_{15} becomes the three-dimensional half-sandwich-shaped structure of PB_{15} after P atom doping; thus, studying the structures and characteristics of PB_{15} is crucial to understanding the structural laws of doped nonmetallic boron clusters. In summary, the study of PB_7 and PB_{15} is of great significance for the discovery of new stable boron-based nanomaterials.

2.2. Relative Stabilities

To analyze the relative stabilities of the lowest energy level of $PB_n^{0/-}$ (n = 3−17), we calculated the average binding energy (E_b) and the second-order energy differences (Δ^2E) of the clusters using the following formulas, where n represents the number of boron atoms, and E is the total energy of the corresponding atom or cluster. The calculation results obtained using Equations (1)–(3) are plotted in Figure 3. The formulas are as follows:

$$E_b(PB_n) = [nE(B) + E(P) - E(PB_n)]/(n + 1) \quad (1)$$

$$E_b(PB_n^-) = [(n - 1)E(B) + E(P) + E(B^-) - E(PB_n^-)]/(n + 1) \quad (2)$$

$$\Delta^2E(PB_n^{0/-}) = E(PB_{n-1}^{0/-}) + E(PB_{n+1}^{0/-}) - 2E(PB_n^{0/-}) \quad (3)$$

E_b represents the inherent stability of the cluster, in that a larger value of E_b denotes higher relative stability. As evidenced in Figure 3, the E_b values of $PB_n^{0/-}$ (n = 3−17) are gradually increasing with the increase in the boron atom number n, indicating that the cluster becomes more and more stable. Furthermore, the E_b values of the anions are overall more sizable than those of the corresponding neutral ions; thus, we can infer that the anion clusters of PB_n^- (n = 3−17) are more stable than their corresponding neutral clusters, and that the excess electrons enhance the stability of the P-doped boron clusters. Δ^2E is an important indicator of relative stability and can provide valuable insights into the stability of the clusters. In Figure 3, the second-order difference of the peaks found in n = 4, 8, 10, 12, 13, 14, 15, and 16 indicate that PB_4^-, PB_8^-, PB_8, PB_{10}^-, PB_{12}^-, PB_{13}, PB_{14}^-, PB_{15}, and PB_{16}^- are relatively more stable than their adjacent clusters.

The energy difference E_{gap} between HOMO and LUMO is an indicator of chemical stability. A larger E_{gap} value for a cluster implies that the electrons are more difficult to excite from HOMO to LUMO, which indicates that the corresponding structures are chemically inert. As can be seen in Figure 3, two obvious E_{gap} peaks are found in PB_7 (about 5.11 eV) and PB_{15} (about 4.31 eV), implying that the neutral clusters PB_7 and PB_{15} exhibit better chemical stability than that of the other clusters. Therefore, combining Δ^2E and E_{gap}

analyses proved that PB_{15} has a high relative and chemical stability. Additionally, due to the PB_7 cluster having the largest values of E_{gap}, as well as a special umbrella structure, we chose these clusters as examples through which to analyze chemical bonding in P-doped boron clusters.

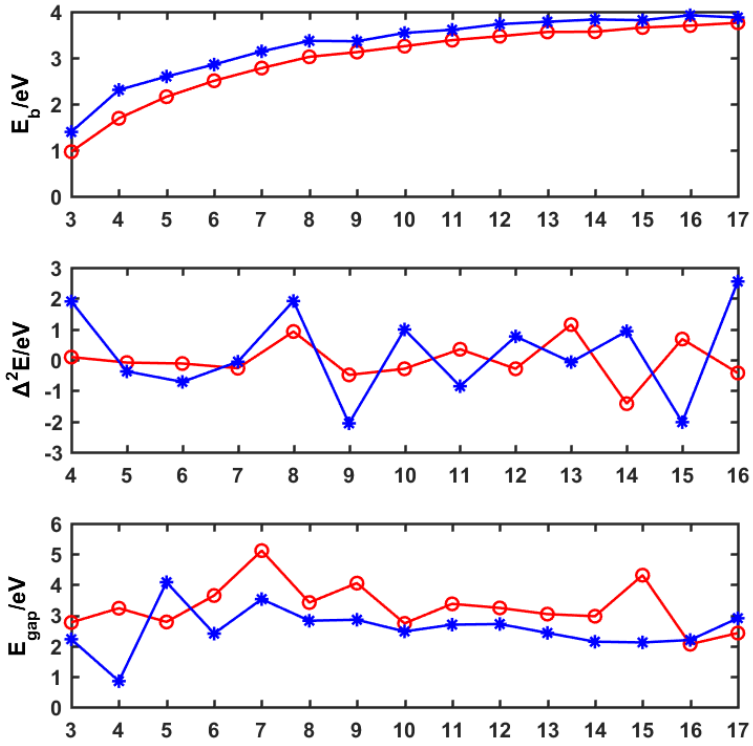

Figure 3. Average binding energy (E_b), second-order energy differences (Δ^2E), and HOMO–LUMO gaps (E_{gap}) of doped boron clusters $PB_n^{0/-}$ (n = 3−17). Red represents the neutral cluster, blue represents the anion cluster, and n represents the number of boron atoms in the cluster.

2.3. Chemical Bonding Analysis

Through a comprehensive stability analysis of all of the clusters detailed in the previous section, we inferred that PB_7 and PB_{15} show chemical stability, due to their high E_{gap} values. We analyzed the charge populations of PB_7 and PB_{15} (see Figure S33). Different from the metal elements in metal-doped boron clusters, which can undergo one or more electron transfers, the phosphorus atom in PB_7 or PB_{15} transfers less than one electron. To further understand the electronic properties and stability of the closed-shell clusters PB_7 and PB_{15}, the AdNDP method was used to analyze their chemical bonding characteristics. The AdNDP method is an extension of the popular natural bond orbital (NBO) analysis, which can be used to analyze localized and delocalized multicenter bonds. We quantitatively analyzed the bonding properties of PB_7 and PB_{15} using the AdNDP method, and the results are depicted in Figures 4 and 5. In Figure 4, we clearly observe six two-center two-electron (2c–2e) σ bonds around the peripheral B atoms of the PB_7 cluster. In addition, there are three 8c–2e σ bonds and three 8c–2e π bonds in PB_7, which together support the plane of the cluster and enhance the stability of PB_7. As can be seen in the Figure 4, the contribution of the P atom to the 8c–2e π bonds is greater than its contribution to the 8c–2e σ bonds. The delocalized σ and π bonds give rise to double aromaticity and fulfill the Hückel 4N + 2 rule with N = 1.

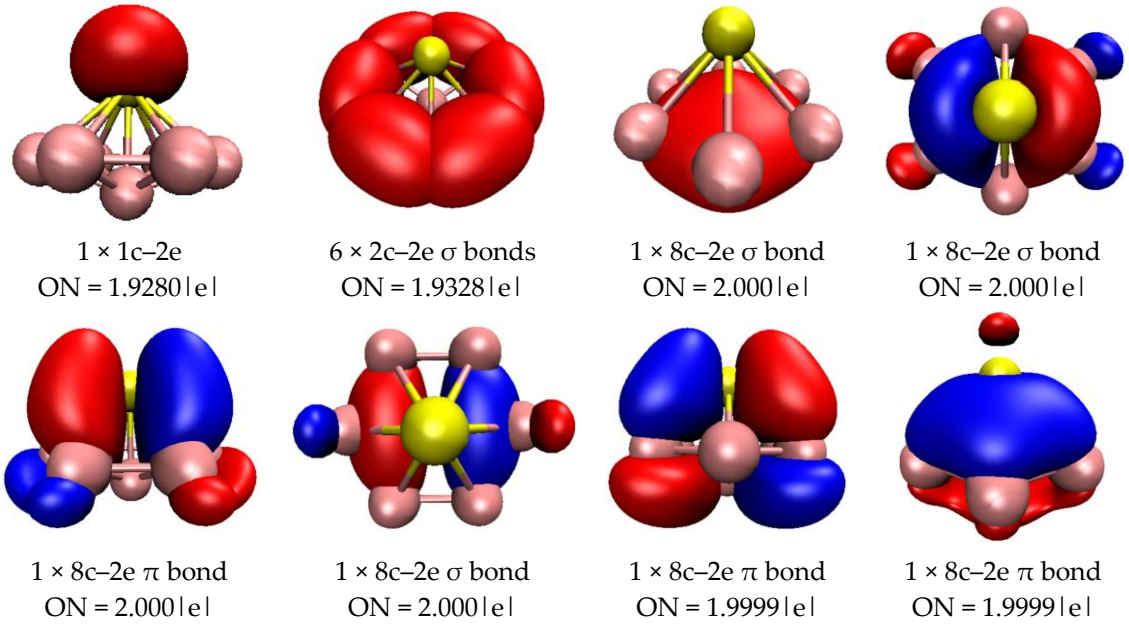

Figure 4. AdNDP analysis of PB_7. ON is the occupation number, and the yellow ball is the P atom.

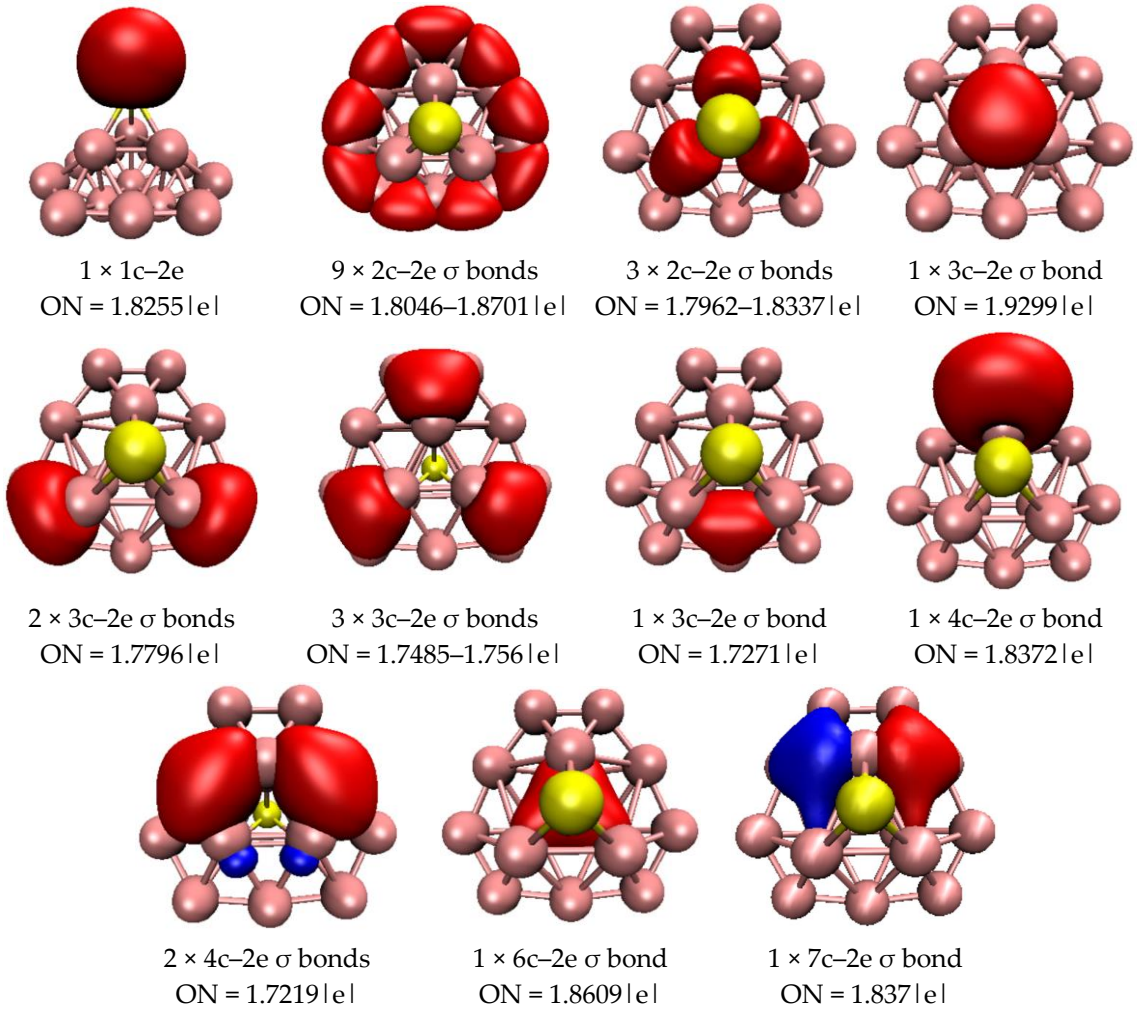

Figure 5. AdNDP analysis of PB_{15}. ON is the occupation number, and the yellow ball is the P atom.

For PB_{15} (Figure 5), there is one lone pair on the P atom, and three 2c–2e σ bonds cover the B–P bond attached to the P atom. These three 2c–2e σ bonds are formed by three electrons on the P atom combining with an electron of each B atom on the B_3 ring. In addition, nine 2c–2e σ bonds are distributed over the peripheral B–B bond. The seven 3c–2e σ bonds are divided into the four following groups: one 3c–2e σ bond is distributed on the inner ring triangle at the back side of the P atom, two 3c–2e σ bonds are distributed on two peripheral B_3 rings, three 3c–2e σ bonds cover the three peripheral B_3 rings behind the P atom, and the last 3c–2e σ bond is distributed on a ternary boron ring. Moreover, there are three 4c–2e σ bonds over three B_4 rings, one 6c–2e σ bond attached to an internal B_6 ring, and one 7c–2e σ bond over a B_7 ring. On the whole, there are strong interactions between B_{15} and the P atom through delocalized bonds that stabilize the PB_{15} cluster. According to AdNDP investigations, the PB_{15} cluster possesses 12 delocalized σ bonds that do not satisfy spherical aromaticity [$2(n + 1)^2$ rule].

To further confirm the above AdNDP analysis results, we analyzed PB_7 and PB_{15} using the ELF method, a function that can be used to describe the localization and delocalization of different molecular regions. The ELF results for PB_7 and PB_{15} are shown in Figure 6, as well as in Figures S31 and S32, respectively. As can be observed from Figure 6 and Figure S31, the isosurface map of PB_7 covers six peripheral B–B bonds that correspond to six peripheral 2c–2e σ bonds, as well as the entire region of B and P atoms corresponding to the 8c–2e bonds. Combining Figure S32 and Figure 6 shows that the isosurface map of PB_{15} covers nine peripheral B–B bonds and three B–P bonds, which correspond to twelve 2c–2e σ bonds, as well as seven B_3 triangles that correspond to seven 3c–2e σ bonds. Additionally, the three regions around PB_{15} are fatter, indicating the presence of 3c–2e and 4c–2e bonds.

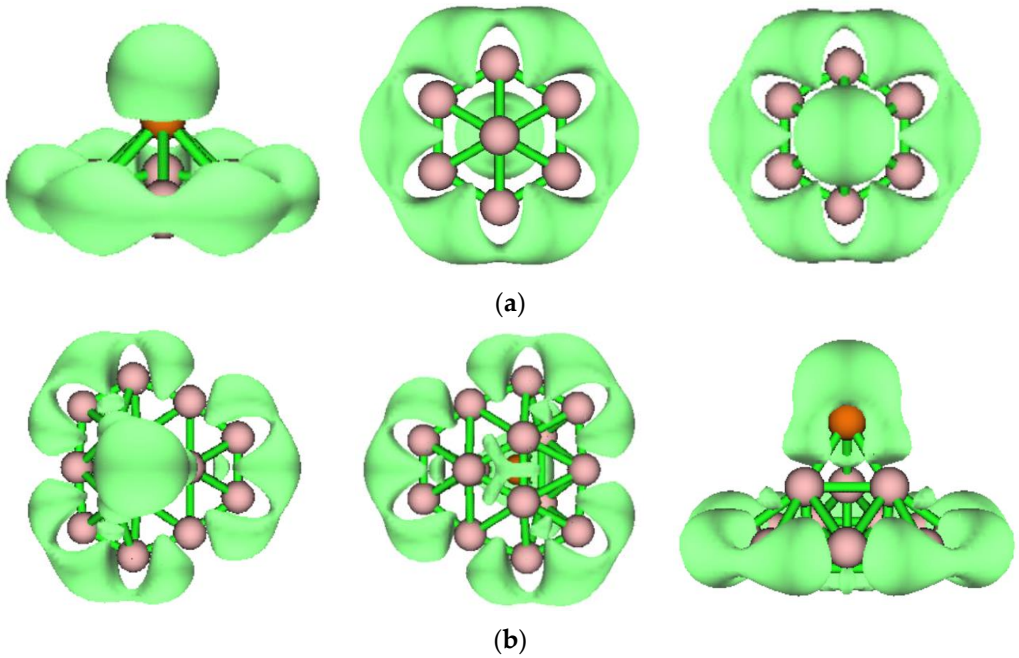

Figure 6. ELF at the PBE0 level. (**a**) C_{6v} PB_7; the isovalue is 0.8. (**b**) C_S PB_{15}; the isovalue is 0.8.

2.4. Photoelectron Spectra

Photoelectron spectra (PES) is an effective approach for exploring the energy levels of valence electrons in nanoclusters. In photoelectron spectra, the positions of the peaks represent the energy differences between the initial and final electronic state after photons absorption. In order to identify the structures of the PB_n^- (n = 3−17) clusters, we calculated the vertical detachment energies (VDEs) of the anionic clusters and simulated the photoelectron spectra of the PB_n^- (n = 3−17) clusters using the time-dependent density functional theory (TD-DFT). The first few peaks of the photoelectron spectrum are commonly used to identify boron clusters [10,15]; thus, studying the peaks on the low-binding-energy side is

of significant importance. Figure 7 shows the photoelectron spectra of the PB_n^- (n = 3–17) clusters. According to the photoelectron spectra, the anion PB_{16}^- exhibits the largest first VDE value (3.88 eV, list in Table S1), while PB_4^- shows the lowest first VDE (1.78 eV). In addition, the energy gap (about 1.95 eV) between the first and second PB_6^- energy bands is the largest.

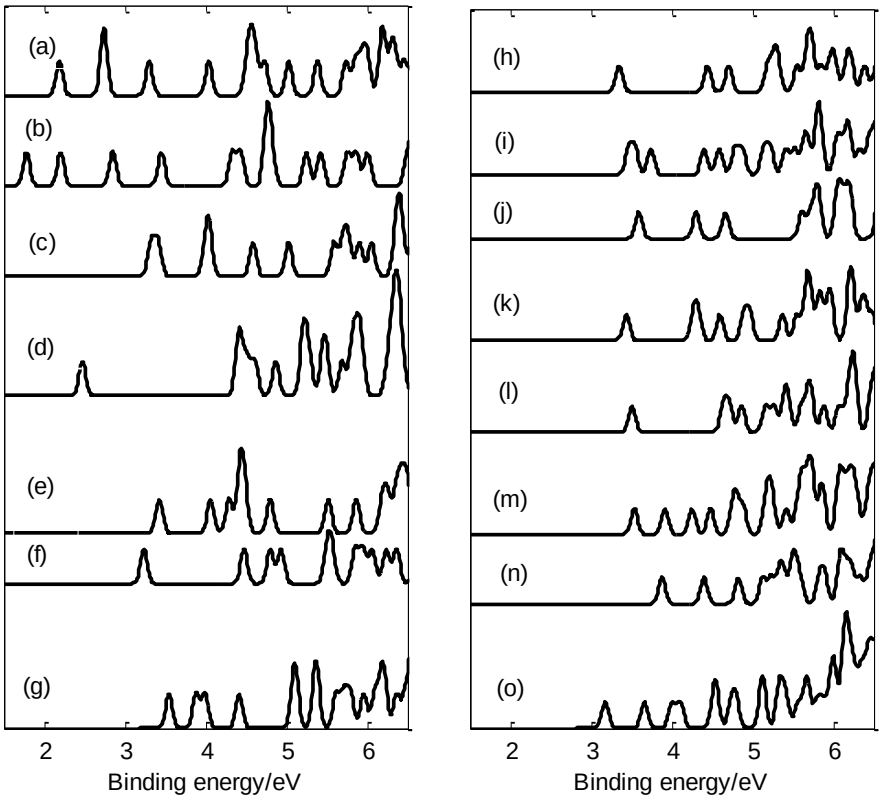

Figure 7. Photoelectron spectra at the PBE0/6-311+G * level: (**a**) PB_3^-; (**b**) PB_4^-; (**c**) PB_5^-; (**d**) PB_6^-; (**e**) PB_7^-; (**f**) PB_8^-; (**g**) PB_9^-; (**h**) PB_{10}^-; (**i**) PB_{11}^-; (**j**) PB_{12}^-; (**k**) PB_{13}^-; (**l**) PB_{14}^-; (**m**) PB_{15}^-; (**n**) PB_{16}^-; (**o**) PB_{17}^-.

The first peaks of the photoelectron spectrum (except for those of PB_4^-, PB_5^- and PB_{11}^-) are derived from the calculated ground-state VDEs of PB_3^-, PB_6^-, PB_7^-, PB_8^-, PB_9^-, PB_{10}^-, PB_{12}^-, PB_{13}^-, PB_{14}^-, PB_{15}^-, PB_{16}^- and PB_{17}^- at 2.19, 2.47, 3.43, 3.24, 3.55, 3.35, 3.59, 3.44, 3.51, 3.53, 3.88, and 3.17 eV, respectively. The first peak of PB_4^- comes from the second VDE (2.2 eV). For open-shell PB_5^- and PB_{11}^-, their first peaks come from the first and second VDEs (3.33 and 3.41 eV for PB_5^-, 3.47 and 3.54 eV for PB_{11}^-). Furthermore, the second peaks of PB_7^-, PB_8^-, PB_9^-, PB_{10}^-, PB_{12}^-, PB_{14}^-, PB_{15}^-, PB_{16}^-, and PB_{17}^- come from the second VDEs at 3.72, 4.06, 4.47, 3.88, 4.44, 4.3, 4.64, 3.9, 4.4, and 3.66 eV, respectively. The second peak of the photoelectron spectrum of PB_4^- comes from the ground-state VDE at 1.78 eV. However, the second peaks of PB_3^-, PB_6^-, and PB_{13}^- are derived from the second and third VDEs (2.736 and 2.744 eV for PB_3^-; 4.4 and 4.43 eV for PB_6^-; 4.27 and 4.33 eV for PB_{13}^-). The second peak of PB_5^- comes from the third VDE (4.01 eV) and the fourth VDE (4.05 eV). For PB_{11}^-, the second peak comes from the third VDE (3.74 eV). Furthermore, peaks with higher binding energies are derived from the separation of electrons from lower molecular orbitals.

Partially anionic boron clusters doped with P atoms have similar structures to those of the corresponding bare boron clusters; however, a comparison of their photoelectron spectra revealed that the addition of a phosphorus atom results in large changes in the photoelectron spectra of most clusters (except for PB_{11}^-) [23,50]. For instance, the doped P atom causes the first peaks of PB_3^-, PB_6^-, and PB_{13}^- to move 0.63, 0.54, and 0.34 eV, respectively, towards the low-binding-energy side. At the same time, the first peaks of

PB_5^-, PB_7^-, PB_8^-, PB_{10}^-, PB_{12}^-, PB_{14}^-, PB_{15}^-, and PB_{16}^- moved 0.93, 0.58, 0.22, 0.29, 1.33, 0.41, 0.1, and 0.49 eV, respectively, to the high-binding-energy side. As can be seen from Figure 7, all photoelectron spectra are different, which indicates that the addition of P atoms not only alters the geometric structure of the clusters, but also leads to changes in their electronic structures. In summary, it is of great significance to study the peaks at the low-binding-energy side, as these simulated spectra may be used as fingerprints with which to identify PB_n^- (n = 3–17) structures in the future.

3. Computation Details

In this paper, the geometrical structure searches for the neutral and anionic clusters of $PB_n^{0/-}$ (n = 3–17) were performed using CALYPSO, an efficient and reliable method for searching for geometrical cluster configurations which has been successfully applied to the study of both boron clusters and doped boron clusters [25,27,33,36,40,54,56–59]. CALYPSO 5.0 software generates 70% of the structure in each generation, and the remaining 30% is formed randomly. When the size of a boron atom is in the range of n = 3–10, nearly 100–1200 isomers are initially obtained for each cluster. The number of isomers increases with the number of boron atoms; when n = 11–14, there are approximately 2000 isomers for each cluster, and when n = 15–17, the number of isomers increases to 2500.

After the initial structural search, the lower energy structures of $PB_n^{0/-}$ (n = 3–17) were optimized at the PBE0/6-311+G(d) level, which is a reliable level for analyzing boron clusters, since the theoretical simulation values (photoelectron spectra) are consistent with the experimental values [15,25,38,59–61]. In order to obtain more accurate relative energy values, we performed CCSD(T) [62] calculations [CCSD(T)/6-311+G(d)//PBE0/6-311+G(d)]+ZPE(zero-point energy corrections) using the optimized PBE0 geometries for the collected isomers. The harmonic frequency and electronic structures were analyzed at the PBE0/6-311+G(d) level; therefore, the calculations below were obtained using the PBE0/6-311+G(d) and CCSD(T)/6-311+G(d)//PBE0/6-311+G(d)+ZPE methods, employing Gaussian16 software [63]. In addition, AdNDP and ELF are implemented in Multiwfn 3.7 software [64], and the AdNDP results were visualized using Visual Molecular Dynamics (VMD) 1.9.3 software [65].

4. Conclusions

In this work, the ground state structures of P-doped boron clusters $PB_n^{0/-}$ (n = 3–17) were identified using the CALYPSO method. In addition, the bonding properties of PB_7 and PB_{15} were discussed, based on AdNDP and ELF analyses, and the photoelectron spectra of the anionic clusters were also calculated. The conclusions can be summarized as follows: (1) The lowest-lying energy structures of PB_n^- (n = 3–17) clusters, except for PB_{17}^-, exhibit planar or quasi-planar structures. The lowest energy structures of PB_n (n = 3–17) are planar or quasi-planar, with the exceptions of PB_7, PB_9, and PB_{15}. The lowest energy structure of PB_7 has an umbrella-like structure, with high symmetry (C_{6V}), and the ground-state configuration of PB_{10}^- exhibits a chiral symmetric structure. (2) The lowest energy structures of the neutral ion PB_{15} have a half-sandwich structure, and they possess relatively high Δ^2E and E_{gap} values, indicating that they possess superior relative and chemical stability. (3) AdNDP bonding analysis and ELF analysis further verified the stability and validity of the lowest energy structures of PB_7 and PB_{15}. (4) The PB_n^- anionic clusters (n = 3–17) exhibit different photoelectron spectra on their low-binding-energy sides, which can provide a theoretical basis for the identification of doped boron clusters.

Supplementary Materials: The following supporting information can be downloaded at: https://www.mdpi.com/article/10.3390/molecules29143384/s1, Figures S1–S30: Low-lying isomers of doped boron clusters $PB_n^{0/-}$ (n = 3–17); Figure S31: Electron localization function (ELF) of PB_7 with the isovalue set to 0.59; Figure S32: Electron localization function (ELF) of PB_{15} with the isovalue set to 0.7; Figure S33: Charge population of PB_7 and PB_{15}; Table S1: The first VDE values of bare B clusters and P-doped boron clusters.

Author Contributions: Conceptualization, S.L. and Y.Y.; methodology, D.W. and S.L.; software, S.L.; investigation, S.L.; data processing, D.W.; writing—original draft preparation, D.W.; writing—review and editing, S.L. and D.W.; funding acquisition, D.C. and Y.Y. All authors have read and agreed to the published version of the manuscript.

Funding: This research was funded by the Central Guiding Local Science and Technology Development Foundation of China (Grant No. QK ZYD [2019]4012), as well as the Growth Foundation for Young Scientists of the Education Department of Guizhou Province (Grant No: QJH KY[2022]310, QJJ [2022]260), China.

Institutional Review Board Statement: Not applicable.

Informed Consent Statement: Not applicable.

Data Availability Statement: The data presented in this study are available in the article and the Supplementary Materials.

Conflicts of Interest: There are no conflicts of interest to declare.

References

1. Harmgarth, N.; Liebing, P.; Lorenz, V.; Engelhardt, F.; Hilfert, L.; Busse, S.; Goldhahn, R.; Edelmann, F.T. Synthesis and Structural Characterization of p-Carboranylamidine Derivatives. *Molecules* **2023**, *28*, 3837. [CrossRef] [PubMed]
2. Diaw-Ndiaye, F.; Sanz Miguel, P.J.; Rodríguez, R.; Macías, R. The Synthesis, Characterization, and Fluxional Behavior of a Hydridorhodatetraborane. *Molecules* **2023**, *28*, 6462. [CrossRef]
3. Das, S.; Shareef, M.A.; Das, B.C. Design and Synthesis of New Boron-Based Benzo[c][1,2,5] oxadiazoles and Benzo[c][1,2,5] thiadiazoles as Potential Hypoxia Inhibitors. *Inorganics* **2023**, *11*, 34. [CrossRef]
4. Teixidor, F.; Núñez, R.; Viñas, C. Towards the Application of Purely Inorganic Icosahedral Boron Clusters in Emerging Nanomedicine. *Molecules* **2023**, *28*, 4449. [CrossRef]
5. Sivaev, I.B.; Bregadze, V.I. *Borane, Carborane and Metallacarborane Anions for Stabilization of Transient and Highly Reactive Intermediates*; World Scientific: Singapore, 2018; Volume 1, pp. 147–203.
6. Iijima, S. Helical microtubules of graphitic carbon. *Nature* **1991**, *354*, 56–58. [CrossRef]
7. Novoselov, K.S.; Geim, A.K.; Morozov, S.V.; Jiang, D.; Zhang, Y.; Dubonos, S.V.; Grigorieva, I.V.; Firsov, A.A. Electric Field Effect in Atomically Thin Carbon Films. *Science* **2004**, *306*, 666–669. [CrossRef] [PubMed]
8. Kroto, H.W.; Heath, J.R.; O'Brien, S.C.; Curl, R.F.; Smalley, R.E. C60: Buckminsterfullerene. *Nature* **1985**, *318*, 162–163. [CrossRef]
9. Zhai, H.; Wang, L.; Alexandrova, A.N.; Boldyrev, A.I. Electronic structure and chemical bonding of B_5^- and B_5 by photoelectron spectroscopy and ab initio calculations. *J. Chem. Phys.* **2002**, *117*, 7917–7924. [CrossRef]
10. Zhai, H.; Kiran, B.; Li, J.; Wang, L.-S. Hydrocarbon analogues of boron clusters--planarity, aromaticity and antiaromaticity. *Nat. Mater.* **2003**, *2*, 827–833. [CrossRef]
11. Chen, Q.; Wei, G.F.; Tian, W.J.; Bai, H.; Liu, Z.P.; Zhai, H.J.; Li, S.D. Quasi-planar aromatic B_{36} and B_{36}^- clusters: All-boron analogues of coronene. *Phys. Chem. Chem. Phys.* **2014**, *16*, 18282–18287. [CrossRef]
12. Boustani, I. Systematic ab initio investigation of bare boron clusters: Determination of the geometryand electronic structures of B_n (n = 2–14). *Phys. Rev. B* **1997**, *55*, 16426–16438. [CrossRef]
13. Kiran, B.; Bulusu, S.; Zhai, H.J.; Yoo, S.; Zeng, X.C.; Wang, L.S. Planar-to-tubular structural transition in boron clusters: B_{20} as the embryo of single-walled boron nanotubes. *Proc. Natl. Acad. Sci. USA* **2005**, *102*, 961–964. [CrossRef] [PubMed]
14. Bean, D.E.; Fowler, P.W. Double Aromaticity in "Boron Toroids". *J. Phys. Chem. C* **2009**, *113*, 15569–15575. [CrossRef]
15. Zhai, H.J.; Zhao, Y.F.; Li, W.L.; Chen, Q.; Bai, H.; Hu, H.S.; Piazza, Z.A.; Tian, W.J.; Lu, H.G.; Wu, Y.B.; et al. Observation of an all-boron fullerene. *Nat. Chem.* **2014**, *6*, 727–731. [CrossRef] [PubMed]
16. Bai, H.; Chen, Q.; Zhai, H.J.; Li, S.D. Endohedral and exohedral metalloborospherenes: M@B_{40} (M = Ca, Sr) and M&B_{40} (M = Be, Mg). *Angew. Chem. Int. Ed.* **2014**, *54*, 941–945.
17. Shakerzadeh, E.; Biglari, Z.; Tahmasebi, E. M@B_{40} (M = Li, Na, K) serving as a potential promising novel NLO nanomaterial. *Chem. Phys. Lett.* **2016**, *654*, 76–80. [CrossRef]
18. An, Y.; Zhang, M.; Wu, D.; Fu, Z.; Wang, T.; Xia, C. Electronic transport properties of the first all-boron fullerene B_{40} and its metallofullerene Sr@B_{40}. *Phys. Chem. Chem. Phys.* **2016**, *18*, 12024–12028. [CrossRef] [PubMed]
19. Tang, C.; Zhang, X. The hydrogen storage capacity of Sc atoms decorated porous boron fullerene B_{40}: A DFT study. *Int. J. Hydrogen Energy* **2016**, *41*, 16992–16999. [CrossRef]
20. Bai, H.; Bai, B.; Zhang, L.; Huang, W.; Mu, Y.W.; Zhai, H.J.; Li, S.D. Lithium-Decorated Borospherene B_{40}: A Promising Hydrogen Storage Medium. *Sci. Rep.* **2016**, *6*, 35518. [CrossRef]
21. Li, S.; Zhang, Z.; Long, Z.; Chen, D. Structures, Stabilities, and Spectral Properties of Endohedral Borospherenes M@$B_{40}^{0/-}$ (M = H_2, HF, and H_2O). *ACS Omega* **2019**, *4*, 5705–5713. [CrossRef]
22. Dong, H.; Hou, T.; Lee, S.T.; Li, Y. New Ti-decorated B_{40} fullerene as a promising hydrogen storage material. *Sci. Rep.* **2015**, *5*, 9952. [CrossRef] [PubMed]

23. Sergeeva, A.P.; Zubarev, D.Y.; Zhai, H.J.; Boldyrev, A.I.; Wang, L.S. A Photoelectron Spectroscopic and Theoretical Study of B_{16}^- and B_{16}^{2-}: An All-Boron Naphthalene. *J. Am. Chem. Soc.* **2008**, *130*, 7244–7246. [CrossRef] [PubMed]
24. Piazza, Z.A.; Hu, H.S.; Li, W.L.; Zhao, Y.F.; Li, J.; Wang, L.S. Planar hexagonal B_{36} as a potential basis for extended single-atom layer boron sheets. *Nat. Commun.* **2014**, *5*, 3113. [CrossRef]
25. Ren, M.; Jin, S.; Wei, D.; Jin, Y.; Tian, Y.; Lu, C.; Gutsev, G.L. NbB_{12}^-: A new member of half-sandwich type doped boron clusters with high stability. *Phys. Chem. Chem. Phys.* **2019**, *21*, 21746–21752. [CrossRef] [PubMed]
26. Jin, S.; Chen, B.; Kuang, X.; Lu, C.; Gutsev, G.L. Structural evolution and electronic properties of medium-sized boron clusters doped with scandium. *J. Phys. Condens. Matter* **2019**, *31*, 485302. [CrossRef] [PubMed]
27. Wei, D.; Ren, M.; Lu, C.; Bi, J.; Maroulis, G. A quasi-plane IrB_{18}^- cluster with high stability. *Phys. Chem. Chem. Phys.* **2020**, *22*, 5942–5948. [CrossRef]
28. Chen, T.T.; Li, W.L.; Chen, W.J.; Yu, X.H.; Dong, X.R.; Li, J.; Wang, L.S. Spherical trihedral metallo-borospherenes. *Nat. Commun.* **2020**, *11*, 2766. [CrossRef] [PubMed]
29. Chen, W.J.; Kulichenko, M.; Choi, H.W.; Cavanagh, J.; Yuan, D.F.; Boldyrev, A.I.; Wang, L.S. Photoelectron Spectroscopy of Size-Selected Bismuth-Boron Clusters: BiB_n^- (n = 6–8). *J. Phys. Chem. A* **2021**, *125*, 6751–6760. [CrossRef] [PubMed]
30. Chen, T.T.; Li, W.L.; Bai, H.; Chen, W.J.; Dong, X.R.; Li, J.; Wang, L.S. ReB_8^- and ReB_9^-: New Members of the Transition-Metal-Centered Borometallic Molecular Wheel Family. *J. Phys. Chem. A* **2019**, *123*, 5317–5324. [CrossRef]
31. Cheung, L.F.; Czekner, J.; Kocheril, G.S.; Wang, L.S. $ReB6^-$: A Metallaboron Analog of Metallabenzenes. *J. Am. Chem. Soc.* **2019**, *141*, 17854–17860. [CrossRef]
32. Cheung, L.F.; Kocheril, G.S.; Czekner, J.; Wang, L.-S. Observation of Möbius Aromatic Planar Metallaborocycles. *J. Am. Chem. Soc.* **2020**, *142*, 3356–3360. [CrossRef]
33. Liang, W.Y.; Das, A.; Dong, X.; Cui, Z.H. Lithium doped tubular structure in LiB_{20} and LiB_{20}^-: A viable global minimum. *Phys. Chem. Chem. Phys.* **2018**, *20*, 16202–16208. [CrossRef]
34. Saha, R.; Kar, S.; Pan, S.; Martinez-Guajardo, G.; Merino, G.; Chattaraj, P.K. A Spinning Umbrella: Carbon Monoxide and Dinitrogen Bound MB_{12}^- Clusters (M = Co, Rh, Ir). *J. Phys. Chem. A* **2017**, *121*, 2971–2979. [CrossRef]
35. Sergeeva, A.P.; Popov, I.A.; Piazza, Z.A.; Li, W.L.; Romanescu, C.; Wang, L.S.; Boldyrev, A.I. Understanding boron through size-selected clusters: Structure, chemical bonding, and fluxionality. *Acc. Chem. Res.* **2014**, *47*, 1349–1358. [CrossRef]
36. Liang, W.; Das, A.; Dong, X.; Wang, M.; Cui, Z. Structural and electronic properties of MB_{22}^- (M = Na, K) clusters: Tubular boron versus quasi-planar boron forms. *New J. Chem.* **2019**, *43*, 6507–6512. [CrossRef]
37. Popov, I.A.; Li, W.L.; Piazza, Z.A.; Boldyrev, A.I.; Wang, L.S. Complexes between planar boron clusters and transition metals: A photoelectron spectroscopy and ab initio study of CoB_{12}^- and RhB_{12}^-. *J. Phys. Chem. A* **2014**, *118*, 8098–8105. [CrossRef] [PubMed]
38. Chen, B.L.; Sun, W.G.; Kuang, X.Y.; Lu, C.; Xia, X.X.; Shi, H.X.; Maroulis, G. Structural Stability and Evolution of Medium-Sized Tantalum-Doped Boron Clusters: A Half-Sandwich-Structured TaB_{12}^- Cluster. *Inorg. Chem.* **2018**, *57*, 343–350. [CrossRef]
39. Chacko, S.; Kanhere, D.G.; Boustani, I. Ab initiodensity functional investigation of B_{24} clusters: Rings, tubes, planes, and cages. *Phys. Rev. B* **2003**, *68*, 035414. [CrossRef]
40. Lv, J.; Wang, Y.; Zhang, L.; Lin, H.; Zhao, J.; Ma, Y. Stabilization of fullerene-like boron cages by transition metal encapsulation. *Nanoscale* **2015**, *7*, 10482–10489. [CrossRef]
41. Yang, Y.J.; Li, S.X.; Chen, D.L.; Long, Z.W. Structural and Electronic Properties of Single-Atom Transition Metal-Doped Boron Clusters MB_{24} (M = Sc, V, and Mn). *ACS Omega* **2021**, *6*, 30442–30450. [CrossRef]
42. Li, S.X.; Yang, Y.J.; Chen, D.L.; Long, Z.W. Structures, and electronic and spectral properties of single-atom transition metal-doped boron clusters MB_{24}^- (M = Sc, Ti, V, Cr, Mn, Fe, Co, and Ni). *RSC Adv.* **2022**, *12*, 16706–16716. [CrossRef] [PubMed]
43. Tuyet Mai, D.T.; Van Duong, L.; Pham-Ho, M.P.; Nguyen, M.T. Electronic Structure and Properties of Silicon-Doped Boron Clusters B_nSi with n = 15–24 and Their Anions. *J. Phys. Chem. C* **2020**, *124*, 6770–6783. [CrossRef]
44. Van Duong, L.; Nguyen, M.T. Electronic structure of the boron fullerene B_{14} and its silicon derivatives $B_{13}Si^+$, $B_{13}Si^-$ and $B_{12}Si_2$: A rationalization using a cylinder model. *Phys. Chem. Chem. Phys.* **2016**, *18*, 17619–17626. [CrossRef]
45. Li, P.F.; Zhai, H.J. Structures and chemical bonding of boron-based $B_{12}O$ and $B_{11}Au$ clusters. A counterexample in boronyl chemistry. *Phys. Chem. Chem. Phys.* **2022**, *24*, 10952–10961. [CrossRef]
46. Li, S.X.; Yang, Y.J.; Chen, D.L. PB_{12}^+ and $P_2B_{12}^{+/0/-}$: The Novel B_{12} Cage Doped by Nonmetallic P Atoms. *ACS Omega* **2023**, *8*, 44831–44838. [CrossRef] [PubMed]
47. Yang, Y.J.; Li, S.X.; Chen, D.L.; Long, Z.W. Structural Evolution and Electronic Properties of Selenium-Doped Boron Clusters $SeB_n^{0/-}$ (n = 3–16). *Molecules* **2023**, *28*, 357. [CrossRef] [PubMed]
48. Lv, J.; Wang, Y.; Zhu, L.; Ma, Y. Particle-swarm structure prediction on clusters. *J. Chem. Phys.* **2012**, *137*, 084104. [CrossRef]
49. Adamo, C.; Barone, V. Toward reliable density functional methods without adjustable parameters: The PBE0 model. *J. Chem. Phys.* **1999**, *110*, 6158–6170. [CrossRef]
50. Alexandrova, A.N.; Boldyrev, A.I.; Zhai, H.J.; Wang, L.S. All-boron aromatic clusters as potential new inorganic ligands and building blocks in chemistry. *Coord. Chem. Rev.* **2006**, *250*, 2811–2866. [CrossRef]
51. Barroso, J.; Pan, S.; Merino, G. Structural transformations in boron clusters induced by metal doping. *Chem. Soc. Rev.* **2022**, *51*, 1098–1123. [CrossRef]

52. Gong, L.F.; Guo, W.L.; Wu, X.M.; Li, Q.S. B_7^- as a novel ligand: Theoretical investigations on structures and chemical bonding of LiB_7 and BeB_7^+. *Chem. Phys. Lett.* **2006**, *429*, 326–334. [CrossRef]
53. Kheshti, T.; Mahdavifar, Z.; Noorizadeh, S. Umbrella-shaped vs planar; evolutionary search for BnQ, Be©BnQ (n = 6–12, Q = 0, −1) clusters. *J. Mol. Liq.* **2021**, *328*, 115389. [CrossRef]
54. Đorđević, S.; Radenković, S. Spatial and Electronic Structures of BeB_8 and MgB_8: How far Does the Analogy Go? *Chem. Phys. Chem.* **2022**, *23*, e202200070. [CrossRef] [PubMed]
55. Zhang, N.; Wang, C.; Wu, Q.; Lan, J.; Chai, Z.; Shi, W. Highly stable actinide(iii) complexes supported by doubly aromatic ligands. *Phys. Chem. Chem. Phys.* **2022**, *24*, 5921–5928. [CrossRef] [PubMed]
56. Lv, J.; Wang, Y.; Zhu, L.; Ma, Y. B_{38}: An all-boron fullerene analogue. *Nanoscale* **2014**, *6*, 11692–11696. [CrossRef] [PubMed]
57. Dong, X.; Jalife, S.; Vasquez-Espinal, A.; Barroso, J.; Orozco-Ic, M.; Ravell, E.; Cabellos, J.L.; Liang, W.Y.; Cui, Z.H.; Merino, G. Li_2B_{24}: The simplest combination for a three-ring boron tube. *Nanoscale* **2019**, *11*, 2143–2147. [CrossRef] [PubMed]
58. Dong, X.; Liu, Y.Q.; Liu, X.B.; Pan, S.; Cui, Z.H.; Merino, G. $Be_4B_{12}^+$: A Covalently Bonded Archimedean Beryllo-Borospherene. *Angew. Chem. Int. Ed.* **2022**, *61*, e202208152. [CrossRef]
59. Tian, Y.; Wei, D.; Jin, Y.; Barroso, J.; Lu, C.; Merino, G. Exhaustive exploration of MgB_n (n = 10–20) clusters and their anions. *Phys. Chem. Chem. Phys.* **2019**, *21*, 6935–6941. [CrossRef]
60. Li, P.; Du, X.; Wang, J.J.; Lu, C.; Chen, H. Probing the Structural Evolution and Stabilities of Medium-Sized $MoBn^{0/-}$ Clusters. *J. Phys. Chem. C* **2018**, *122*, 20000–20005. [CrossRef]
61. Jin, S.; Chen, B.; Kuang, X.; Lu, C.; Sun, W.; Xia, X.; Gutsev, G.L. Structural and Electronic Properties of Medium-Sized Aluminum-Doped Boron Clusters AlB_n and Their Anions. *J. Phys. Chem. C* **2019**, *123*, 6276–6283. [CrossRef]
62. Bartlett, R.J.; Musiał, M. Coupled-cluster theory in quantum chemistry. *Rev. Mod. Phys.* **2007**, *79*, 291–352. [CrossRef]
63. Frisch, M.J.; Trucks, G.W.; Schlegel, H.B.; Scuseria, G.E.; Robb, M.A.; Cheeseman, J.R.; Scalmani, G.; Barone, V.; Petersson, G.A.; Nakatsuji, H.; et al. *Gaussian 16*; Gaussian Inc.: Wallingford, CT, USA, 2016.
64. Lu, T.; Chen, F. Multiwfn: A multifunctional wavefunction analyzer. *J. Comput.Chem.* **2012**, *33*, 580–592. [CrossRef] [PubMed]
65. Humphrey, W.; Dalke, A.; Schulten, K. VMD: Visual molecular dynamics. *J. Mol. Graph.* **1996**, *14*, 33–38. [CrossRef] [PubMed]